Beyond Traditional Poincaré Analysis: Second-Order Plots Reveal Respiratory Effects in Heart Rate Variability

Mikhail A Lebedev[1,2,*], Alexandra S Medvedeva[3], Ksenia P Solovieva[3,4], Nadezhda M Starodubtseva[4], Anna V Makarova[3], Daria F Kleeva[3,4]

[1]Faculty of Mechanics and Mathematics, Lomonosov Moscow State University

[2]Sechenov Institute of Evolutionary Physiology and Biochemistry of the Russian Academy of Sciences

[3]MSU Institute for Artificial Intelligence, Lomonosov Moscow State University

[4]Institute for Information Transmission Problems of the Russian Academy of Sciences

[*]Corresponding author: mikhail.a.lebedev@gmail.com

Abstract

Poincaré plots are commonly used to visualize and quantify the most rapid component of heart rate variability (HRV), capturing the interdependence of successive beat-to-beat intervals. In this study, the analysis was enhanced by introducing the second-order Poincaré plot, where axes represented interval increments rather than consecutive intervals. Using data from healthy subjects at rest and during classical music listening, it was demonstrated that this method filtered out the elliptical shape observed in traditional Poincaré plots, which reflected slow HRV, thereby emphasizing faster variability. Ring-shaped patterns emerged in the plots for several participants, indicating heart rate correlation with respiratory cycles. For the other subjects, the plots displayed point clouds with positive, negative, or no serial correlation. Further analysis revealed that positive correlation arose during slow breathing, while negative correlation occurred with rapid breathing, corresponding to the ratio between respiratory frequency and heart rate. A simple oscillator model—consisting of a fast (cardiac)

oscillator modulated by a slow (respiratory) oscillator—confirmed these findings. Although the study is primarily focused on HRV, the second-order Poincaré plot holds potential for broader applications in physiological and neurophysiological signal analysis.

Introduction

Heart rate variability (HRV) reflects the dynamic interplay between sympathetic and parasympathetic nervous system activity, offering valuable insights into the heart's adaptive responses to physiological and psychological demands (Shaffer and Ginsberg 2017). As a non-invasive marker, HRV has been extensively utilized in assessing cardiovascular health (Grässler et al. 2021), stress reactivity (Kim et al. 2018), and emotional processing (Lane et al. 2009). Clinically, diminished HRV has been repeatedly linked to adverse health outcomes (Lombardi 2002), while its applications have expanded beyond cardiology to serve as a meaningful biomarker in mental health research (Kemp and Quintana 2013). The advent of wearable technology has further revolutionized HRV monitoring, facilitating continuous, real-time tracking that supports both clinical diagnostics and personal wellness initiatives (Dalmeida and Masala 2021; Li et al. 2023).

HRV analysis utilizes diverse methodologies, including time-domain and frequency-domain techniques, each providing unique perspectives on autonomic nervous system modulation (Shaffer and Ginsberg 2017). These analytical approaches evaluate autonomic regulation across different temporal scales, with the most rapid variations detected through the examination of consecutive heartbeat intervals, known as RR intervals (Calabrese and Lambert-Lacroix 2025; Tateno and Glass 2001; Tsipouras et al. 2005). Among the established parameters for quantifying RR interval variability, researchers commonly employ the root mean square of successive differences (RMSSD) (Ciccone et al. 2017; Munoz et al. 2015) and the count of interval pairs differing by more than a specified threshold, such as 50 milliseconds (NN50) (Mietus et al. 2002).

The pioneering work of Raetz et al. (1991) first introduced Poincaré plots as a tool to examine the dynamic relationship between consecutive RR intervals during different sleep-wake states in felines. Their application of this technique successfully uncovered distinct heartbeat correlation patterns associated with varying physiological states. Following this foundational study, Poincaré plot analysis has evolved into a widely accepted methodology for assessing heart rate variability (Khandoker et al. 2013). The technique's characteristic elliptical distribution of data points yields two clinically relevant parameters: SD1, which quantifies the plot's perpendicular dispersion and captures parasympathetically-mediated instantaneous beat-to-beat variations, and SD2, measuring longitudinal dispersion that reflects combined sympathetic and parasympathetic influences on longer-term heart rate dynamics (Brennan et al. 2002; Tulppo et al. 1996; Voss et al. 2009). These complementary metrics provide a comprehensive view of autonomic nervous system regulation of cardiac activity.

This study presents an advancement in Poincaré analysis through the development of second-order Poincaré plots, offering deeper insights into the dynamics of heart rate variability. Unlike the first-order plot, which examine the relationship between consecutive RR intervals (RR_i vs. RR_{i+1}), our approach analyzes the interdependence of successive

interval differences (ΔRR_i vs. ΔRR_{i+1}). When applied to simultaneous electrocardiographic (ECG) and respiratory recordings from 20 healthy subjects, this technique uncovered distinct, respiration-modulated patterns in HRV, each exhibiting subject-specific features. To explain these observations, we developed a model based on coupled oscillators, where a fast cardiac rhythm is dynamically influenced by a slower respiratory drive.

Methods

In this analysis, we used an open-access dataset “Combined measurement of ECG, Breathing, and Seismocardiograms DataBase” from PhysioNet (Goldberger et al. 2000). The dataset was contributed by Miguel Angel Garcia Gonzalez and Ariadna Argelagos Palou of the Universitat Politecnica de Catalunya (García-González et al. 2013). The dataset comprises recordings from 20 presumed healthy participants. This database was created with two primary objectives: first, to investigate whether subtle errors in RR interval detection—when measured across two different ECG leads—are influenced by respiratory activity; and second, to compare RR intervals derived from standard ECG measurements with surrogate estimates obtained from seismocardiograms (SCG), with the additional goal of optimizing beat-detection algorithms for SCG signals. Data acquisition was performed using a Biopac MP36 system (Santa Barbara, CA, USA). Two channels recorded ECG with a bandwidth of 0.05–150 Hz, while the third channel captured respiratory signals via a thoracic piezoresistive band (Biopac SS5LB sensor, 0.05–10 Hz bandwidth). The fourth channel acquired SCG signals using a triaxial accelerometer (LIS344ALH, ST Microelectronics) with a 0.5–100 Hz bandwidth. ECG electrodes (3M Red Dot 2560) were used with foam tape and conductive gel. All signals were sampled at 5 kHz. Measurements were conducted while participants remained awake and motionless in a supine position on a standard bed. Following sensor placement, baseline recordings were acquired during a 5-minute resting period. Subsequently, subjects listened to classical music for approximately 50 minutes, followed by a final 5-minute.

In this study, we analyzed two 200-second epochs—one during rest and another during music listening—which provided sufficient data for our investigation. Signal processing and computational analyses were performed using custom scripts developed in GNU Octave. The analytical procedure began with selecting the higher-quality ECG channel for each subject (Fig. 1A). Following R-peak detection and timestamping, we examined sequences of four consecutive peaks, corresponding to the time points t_i, t_{i+1}, t_{i+2}, and t_{i+3}. These time markers enabled the calculation of both successive RR intervals (RR_i and RR_{i+1}) and their differences (ΔRR_i and ΔRR_{i+1}). Using these derived measures, we generated conventional Poincaré plots (RR_i versus RR_{i+1}; Fig. 1B) alongside novel second-order Poincaré plots (ΔRR_i versus ΔRR_{i+1}; Fig. 1C) to characterize heart rate variability dynamics.

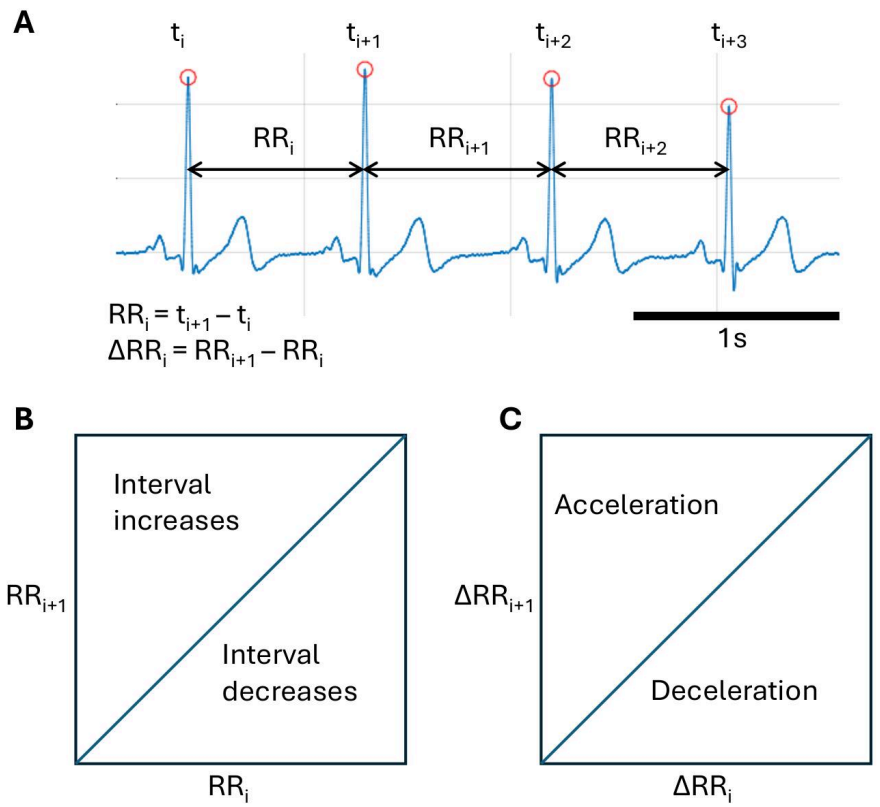

Figure 1. Construction of the first-order and second-order Poincaré plots. A: ECG trace with detected R peaks marked by red circles. Four consecutive peaks are timestamped, and their occurrence times are used to compute RR intervals and successive differences (ΔRR). B: First-order Poincaré plot with RR_i on the x-axis and RR_{i+1} on the y-axis. Points above the line y = x indicate RR interval lengthening, while points below the line indicate shortening. C: Second-order Poincaré plot with ΔRR_i on the x-axis and ΔRR_{i+1} on the y-axis. Points above the line y = x correspond to RR interval acceleration (ΔR increase), while points below the line indicate deceleration (ΔR decrease).

Results

Figure 2 presents the analysis for three participants from the dataset, with blue dots indicating resting states and red dots representing periods of listening to music. For each participant, RR and ΔRR were calculated and plotted as a function of time (Fig. 1A, C, E). The plots for RR reveal very slow heart rate fluctuations (~0.02 Hz), which are attenuated when transitioning to ΔRR. In the classical Poincaré plots (Fig. 1B, D, F, top), a characteristic ellipse is present, with its major axis aligned along the line y = x, reflecting slow variations in RR. The second-order Poincaré plots (Fig. 1B, D, F, bottom) reveal additional patterns not evident in the first-order plots. Notably, participant 3 (Fig. 1B, bottom) exhibits a ring-like structure in these plots, observable during both resting and music-listening conditions. This feature is absent in the other two participants. For participant 9 (Fig. 1D, bottom), the points cluster along the line y = x, indicating positive serial correlation in ΔRR values, with similar patterns in both conditions. In contrast, participant 19 (Fig. 1F, bottom) shows a point distribution perpendicular to the line y = x, reflecting negative serial correlation in ΔRR. This

negative correlation persists across both resting and music-listening states. Importantly, none of these distinct patterns could have been anticipated from the first-order Poincaré plots alone.

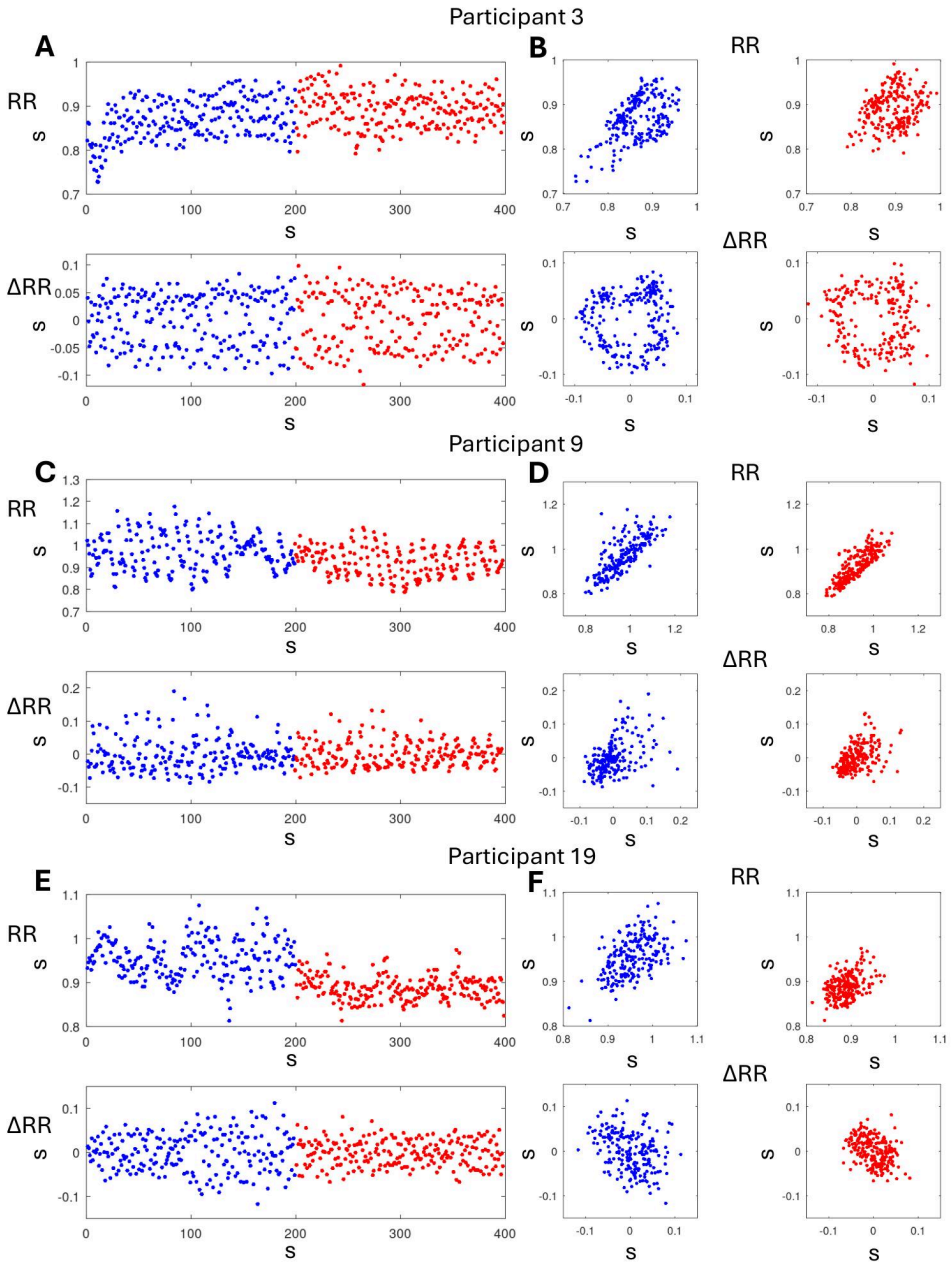

Figure 2. Time course of heartbeat intervals (RR) and their changes (ΔRR), along with first-order and second-order Poincaré plots for the same data. Blue dots indicate resting states, while red dots correspond to listening to music. A, C, E: RR (top) and ΔRR (bottom) plotted over time for participants 3, 9, and 19, respectively. B, D, F: First-order (top) and second-order (bottom) Poincaré plots for the corresponding participants.

The ring-like pattern observed in the second-order Poincaré plot for participant 3, as well as in six other participants upon visual inspection, suggested that the respiratory cycle might be the primary driver of this effect. To investigate this possibility, we examined the modulations

of RR intervals and their changes, ΔRR, in relation to recorded breath patterns. Figure 3 presents the analysis for participant 3, with respiratory recordings aligned to peak inhalation at the top of panels A and B. The corresponding traces for RR intervals and ΔRR are displayed in the middle and bottom sections of these panels, respectively. To facilitate comparison, the discrete data points derived from R peaks were converted into a continuous representation through interpolation. Additionally, panels C through F in Figure 3 illustrate the first-order and second-order Poincaré plots as three-dimensional visualizations, with time represented along the third axis. In this format, the Poincaré plots for both RR and ΔRR form spirals, with each full rotation corresponding to a complete respiratory cycle. These patterns remain consistent between the resting state, depicted in blue, and the music-listening condition, shown in red.

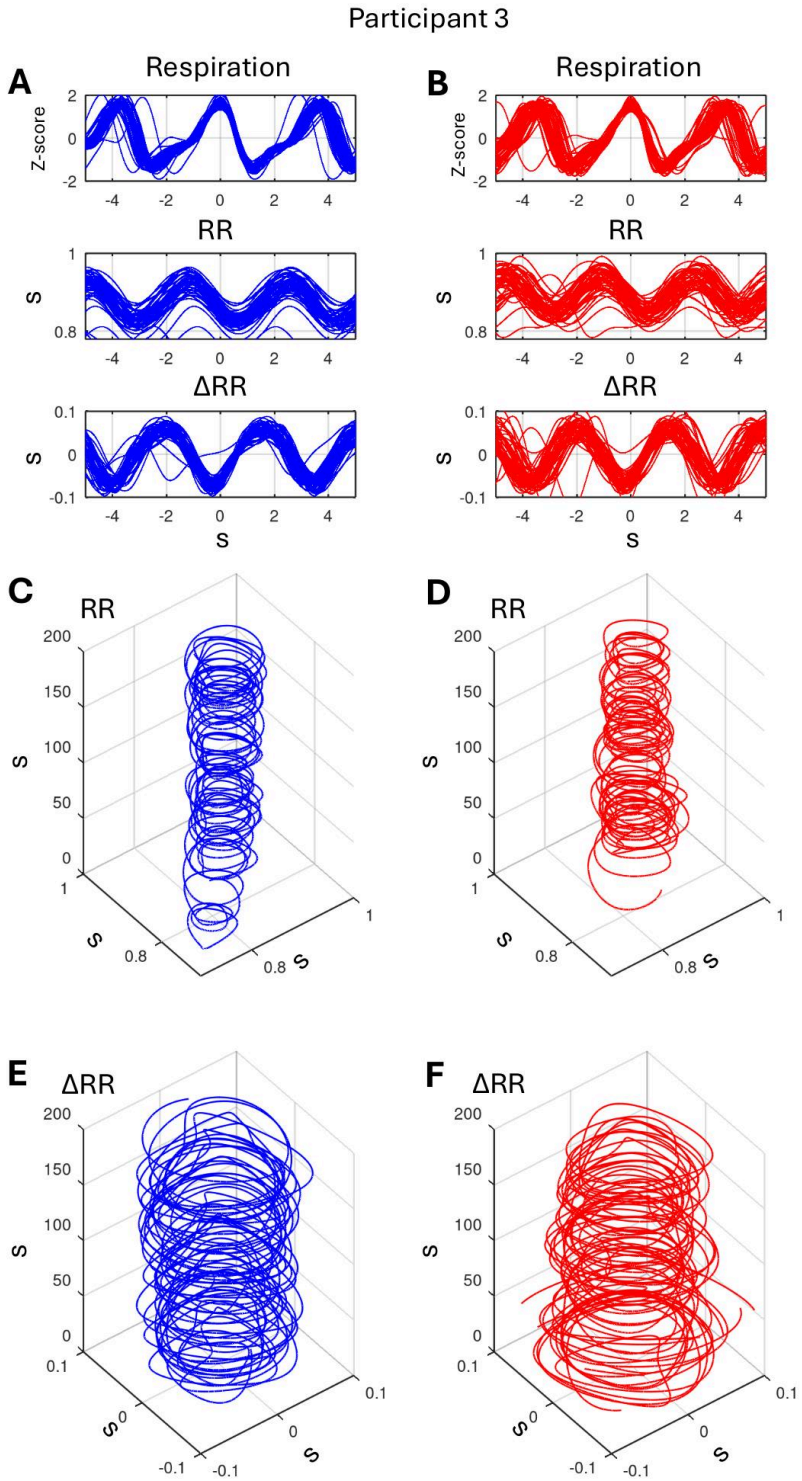

Figure 3. Comparison of respiratory cycles with modulations of RR intervals and ΔRR in participant 3. RR and ΔRR values were interpolated to generate continuous traces, with resting and music-listening conditions depicted in blue and red, respectively. A, B: Respiratory traces (top) aligned to peak inhalation, with corresponding RR (middle) and ΔRR (bottom) modulations. C-F: Three-dimensional representations of first-order (C, D) and second-order (E, F) Poincaré plots, with time as the third axis. Spiral patterns reflect respiratory cycles.

The analysis of Figure 3, which primarily applies to cases with ring-like patterns in second-order Poincaré plots, was supplemented by cross-spectral analyses. In these analyses, cross-spectra were computed for respiration versus ΔRR, the latter treated as a continuous variable. Auto-spectra for both respiration and ΔRR were also calculated. This approach clearly identified spectral peaks corresponding to respiratory cycles. Spectral analyses were similarly performed on ECG records, revealing peaks associated with heart rate. These results demonstrated that the ~1-Hz cardiac oscillator was modulated by a slower secondary frequency of ~0.3 Hz. Figure 4 presents these findings for the same participants as in Figure 2. The figure includes second-order Poincaré plots (Fig. 4A, D, G), spectra for ΔRR and respiration (Fig. 4B, E, H), and ECG spectra (Fig. 4C, F, I). The coefficient of serial correlation, r, was calculated and displayed for the second-order Poincaré plots. Notably, respiration-related spectral peaks were observed not only in the case with the ring pattern (Participant 3, Fig. 4A–C) but also in cases with positive (Participant 9, Fig. 4D–F) and negative (Participant 19, Fig. 4G–I) ΔRR serial correlation. Additional examples of spectral analyses are provided in Figures 5, 6, and 7, corresponding to ring patterns, positive serial correlation, and negative serial correlation, respectively.

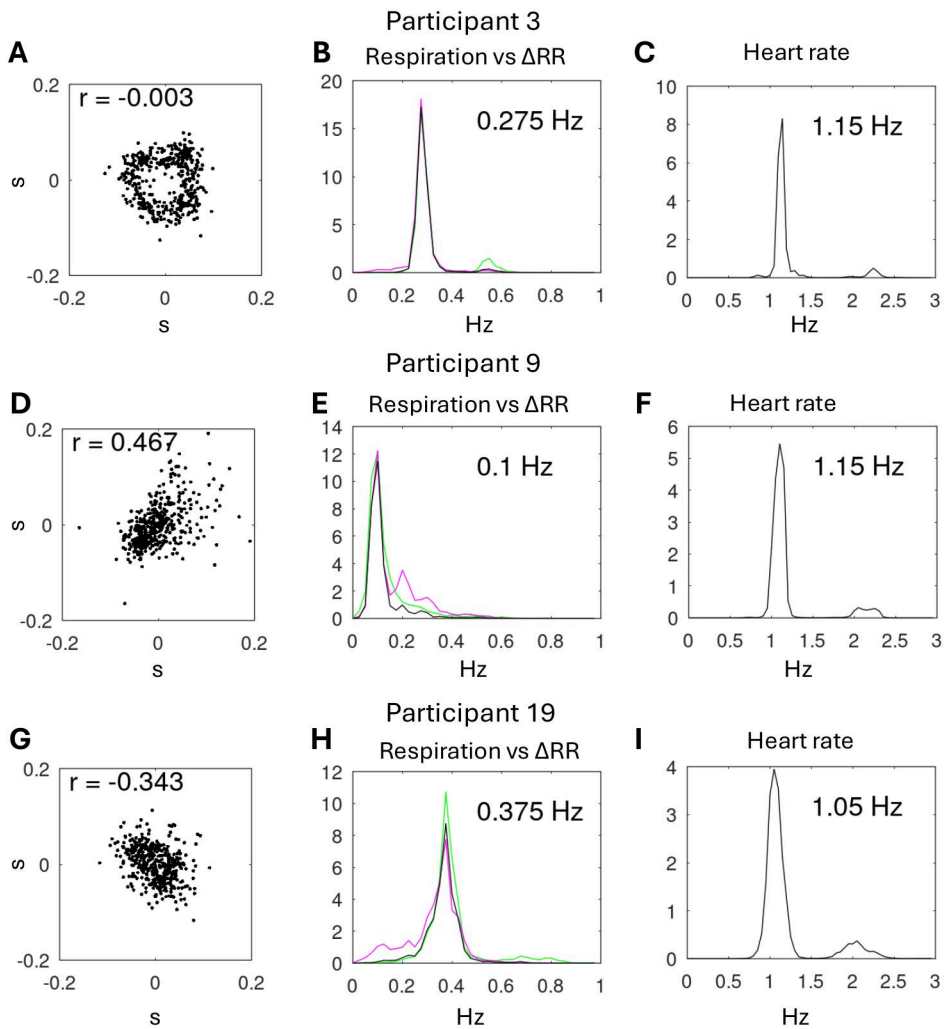

Figure 4. Spectral analysis of heart rate versus respiration. Results are shown for the same participants (3, 9, and 19) as in Figure 2. Data for resting and listening to music are combined. A, D, G: Second-order Poincaré plots, with the coefficient of serial correlation, r,

indicated. B, E, H: Cross-spectral analysis of respiratory-related modulations. Black lines represent cross-spectra (ΔRR vs. respiration), while colored lines denote auto-spectra (green: respiration vs. respiration; magenta: ΔRR vs. ΔRR). Frequencies corresponding to the peaks of ΔRR–respiration cross-spectra are labeled. C, F, I: ECG spectra, with peaks corresponding to heart rate.

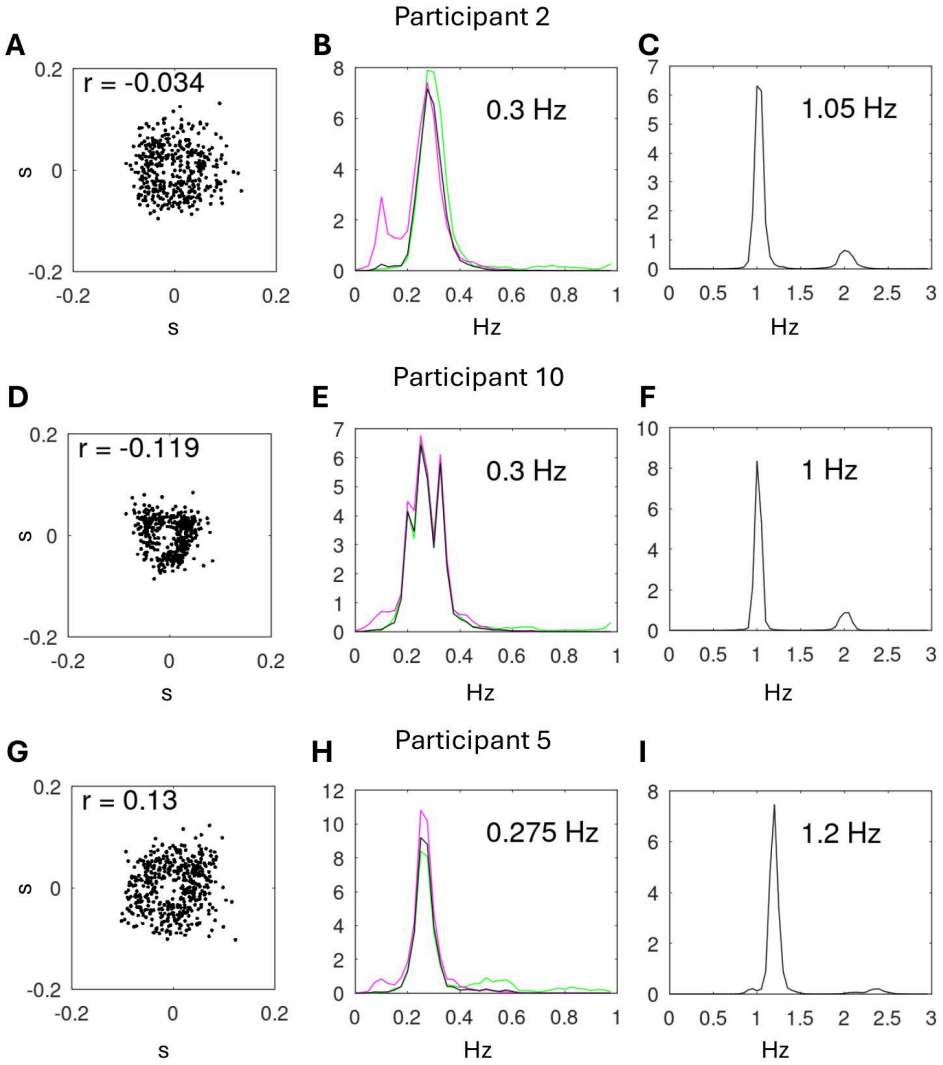

Figure 5. Spectral analysis of heart rate versus respiration for three participants with ring-like patterns in the second-order Poincaré plots. Conventions as in Figure 4.

Figures 4-7 reveal several cases that deviate from the ideal correlation between heart rate and respiration. First, irregular respiration patterns are evident as broad peaks in the respiration autospectra (green lines), as seen in Figs 6B and 7E. Second, ΔRR autospectra (magenta lines) in some cases exhibit modulatory frequencies higher than the breathing rate, such as in Figs 4E, 6B, and 7B,E. Third, even when heart rate and respiration are strongly correlated, variability in respiration rate can broaden the cross-spectrum peak, as illustrated in Fig. 5E. While a detailed analysis of these cases is beyond the scope of this discussion, they may warrant further investigation, particularly in clinical applications.

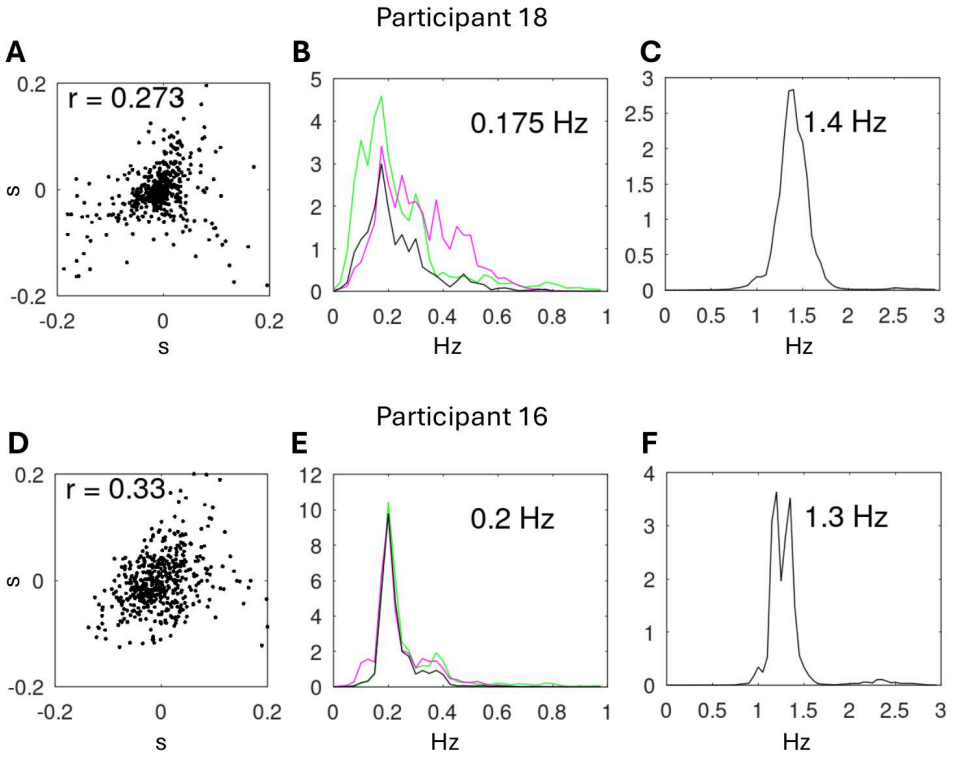

Figure 6. Spectral analysis of heart rate versus respiration for two participants with positive serial correlation in the second-order Poincaré plots. Conventions as in Figure 4.

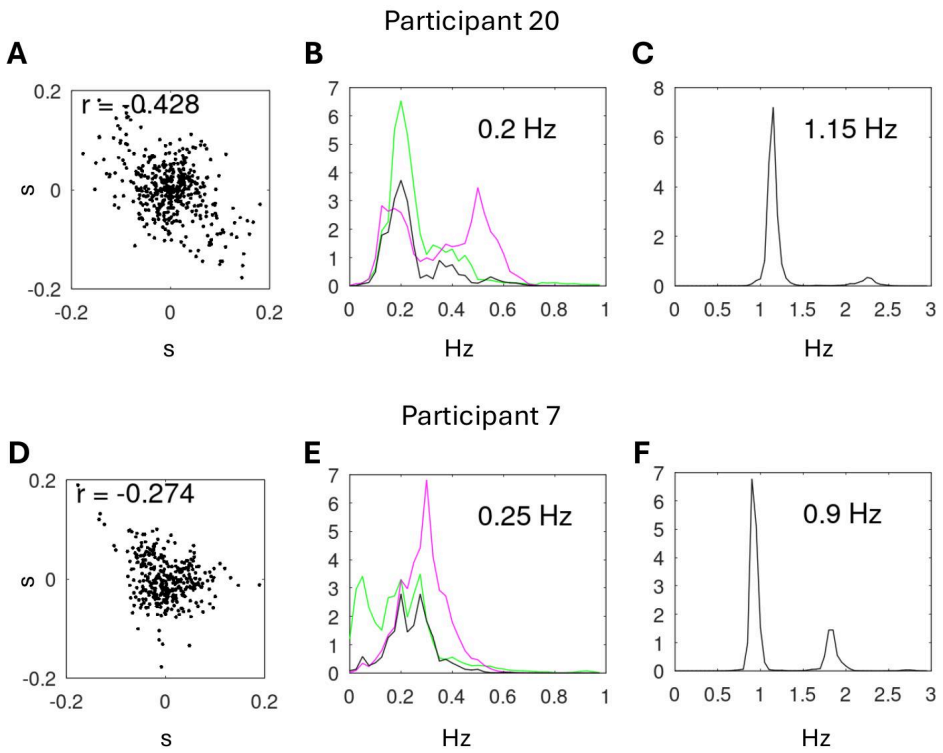

Figure 7. Spectral analysis of heart rate versus respiration for two participants with negative serial correlation in the second-order Poincaré plots. Conventions as in Figure 4.

To summarize the results obtained thus far, we found that second-order Poincaré plots provided additional insights compared to first-order plots. These plots highlighted rapid modulations of RR intervals, contrasting with the slow modulations captured by the first-order plot ellipse. In some cases, they also revealed ring-like patterns associated with a strong correlation between ΔRR and breath cycles. Additionally, they exposed either positive or negative serial correlations in ΔRR, depending on the case. The reason for this variability in serial correlation remains unclear, though a trend emerged: lower breath rates tended to coincide with positive serial correlation, while higher breath rates aligned with negative serial correlation. For instance, participant 9 exhibited positive serial correlation (r = 0.47, Fig. 4D) alongside a low breath rate (0.1 Hz, Fig. 4E), whereas participant 19 showed negative serial correlation (r = -0.34, Fig. 4G) with a higher breath rate (0.38 Hz, Fig. 4H). This pattern persisted across multiple subjects. Thus, participants 9, 16, and 18 displayed positive serial correlations with breath-ΔRR coupling frequencies of 0.1, 0.2, and 0.18 Hz, respectively. In contrast, participants 7, 19, and 20 exhibited negative serial correlations with frequencies of 0.25, 0.38, and 0.2 Hz. Notably, the former group also tended to have higher heart rates (1.15, 1.3, and 1.4 Hz) compared to the latter (0.9, 1.05, and 1.15 Hz). This observation suggests that the coefficient of serial correlation in second-order Poincaré plots could be influenced by the interaction between heart rate and breath rate modulation.

Indeed, when considering the interaction between a high-frequency cardiac oscillator (generating pulses roughly every 1 s) and a low-frequency respiratory oscillator (whose cycle spans approximately 3 heartbeats), altering the rate of either oscillator changes the number of RR intervals within each respiratory cycle. If the respiratory rate slows—and/or the heart rate increases—more RR intervals will fit into a single breath cycle. In such cases, ΔRR tends to follow a pattern where it increases (or decreases) progressively over the course of the respiratory cycle, leading to a positive serial correlation in ΔRR. Conversely, if the respiratory rate increases—and/or the heart rate decreases—fewer RR intervals occur within each breath cycle. As a result, the respiratory cycle becomes too short to sustain a consistent directional change in ΔRR, causing fluctuations that instead produce a negative serial correlation.

To verify whether this mechanism applied to our data, we examined the relationship between the breath-to-heart rate ratio (a measure proportional to the number of RR intervals per respiratory cycle) and the ΔRR serial correlation coefficient, as shown in Fig. 8. The figure presents two variants of this analysis. Figure 8A uses the respiratory frequency derived from cross-spectral analysis (representing the frequency at which respiration modulates ΔRR), while Figure 8B uses the dominant modulation frequency obtained from the ΔRR auto-spectrum, independent of breathing rate. As noted earlier, these frequencies typically coincided when respiratory modulation of heart rate was strong. However, discrepancies arose in certain cases due to additional non-respiratory heart rate modulations or questionable respiratory signal quality. This justified the inclusion of Fig. 8B's analysis, which becomes particularly relevant when respiratory recordings are unavailable. For both analyses, data were segmented into 100-second epochs (yielding two epochs per resting condition and two for music listening), with condition-specific coloring. Regression analysis confirmed our hypothesis in both cases, though the fit was stronger when using the modulation frequency derived solely from the ΔRR spectrum.

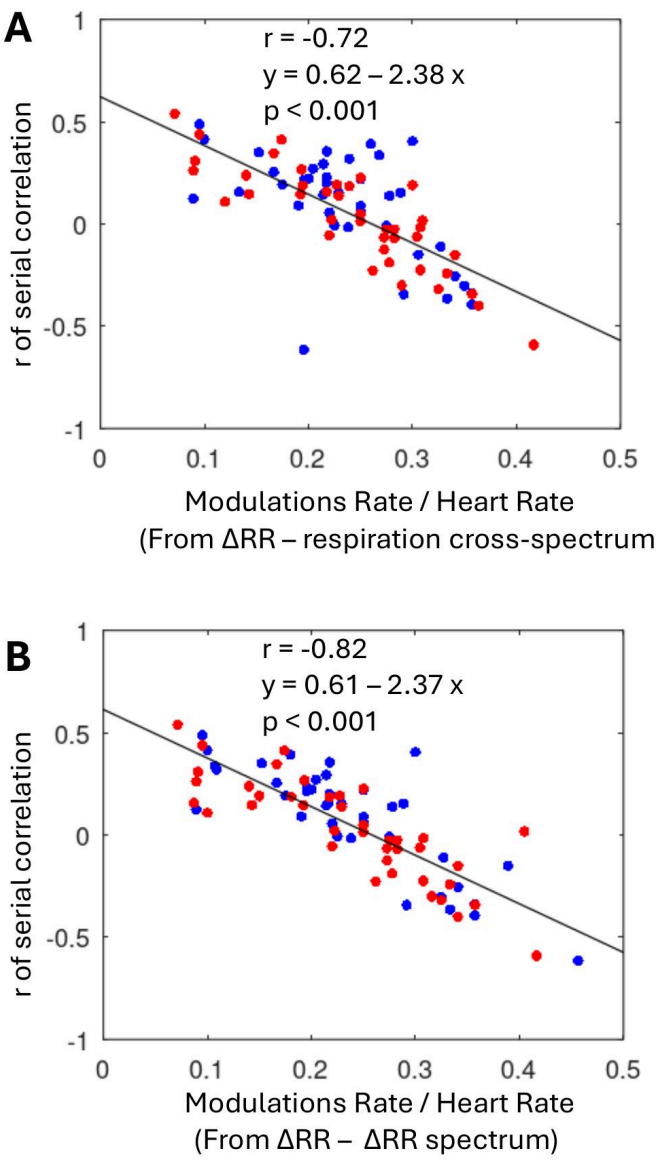

Figure 8. Relationship between modulation frequency-to-heart rate ratio (x-axis) and ΔRR serial correlation coefficient (y-axis). Each data point represents a 100-s recording epoch (blue: resting condition, red: music listening). Solid lines show linear regression fits with corresponding equations (y = ax + b), correlation coefficients (r), and p-values indicated. A: Modulation frequency obtained from cross-spectral analysis of respiration and ΔRR.
B: Modulation frequency obtained from spectral analysis of ΔRR alone.

To further verify the proposed mechanism of negative versus serial correlation in ΔRR for different breathing and heart rates, we developed a simple model of the coupling bewteen an approximately 1 Hz cardiac oscillator with an approximately 0.3 Hz respiratory oscillator (Fig. 9). The cardiac oscillator was modeled using an integrate-and-fire mechanism with a constant rate of rise but a randomly fluctuating starting point (Fig. 9A). An impulse was generated when the integrated rate reached a threshold that was sinusoidally modulated according to the breathing rate. The model successfully reproduced the expected relationship between the ratio of respiration rate to heart rate, which was accurately described by a linear fit (Fig. 9B). Figure 9C displays second-order Poincaré plots for

different model parameters, illustrating a transition from positive to negative serial correlation as breathing rate increased and/or heart rate decreased. Intermediate parameter settings also revealed distinct ring-like patterns, further supporting the model's ability to capture the observed dynamics.

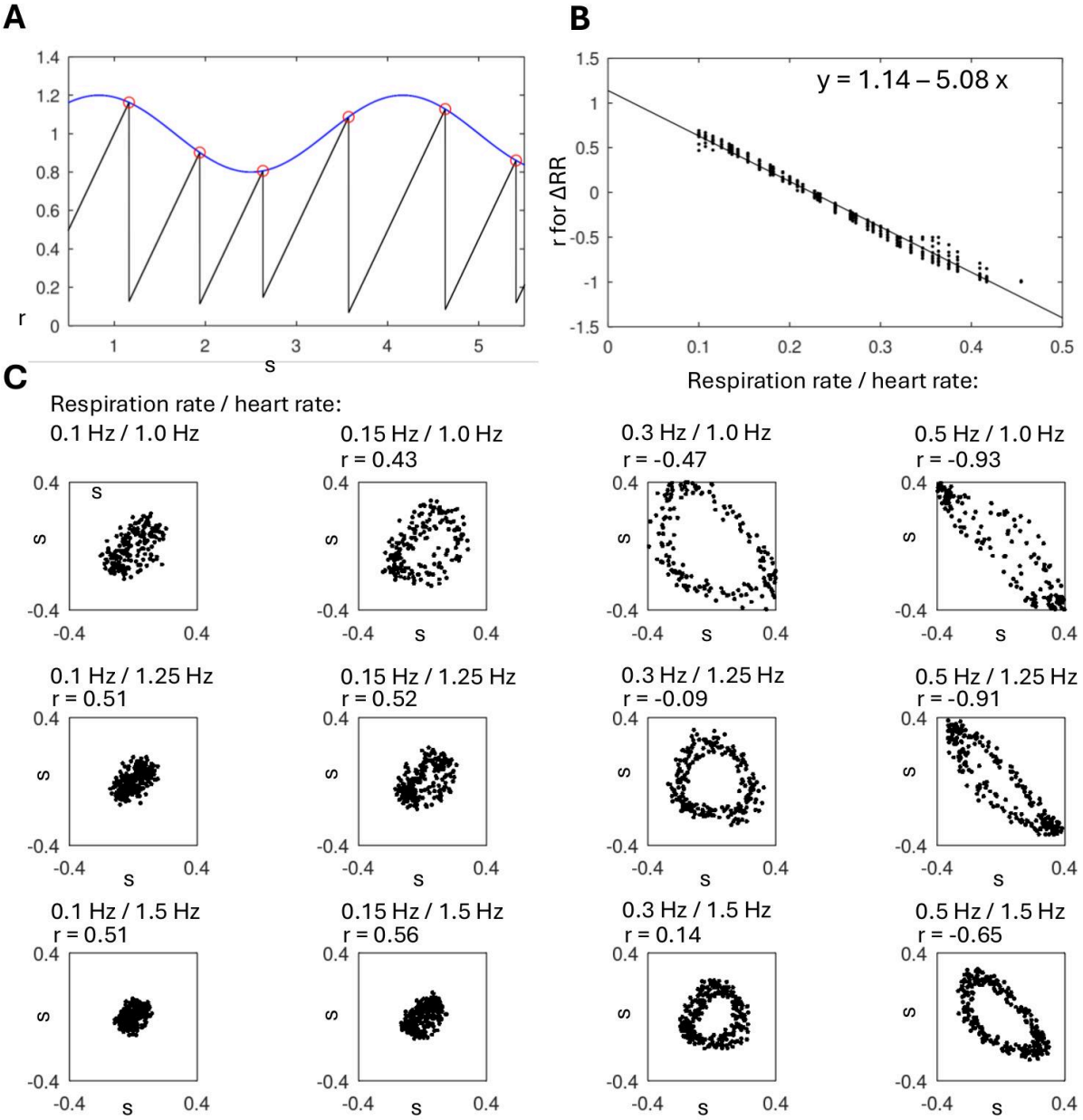

Figure 9. A simple model of coupling between a fast cardiac oscillator (~1 Hz) and a slow respiratory oscillator (~0.3 Hz). A: The cardiac oscillator was modeled as an integrate-and-fire pacemaker with a constant rate of rise but a randomly varying starting point. Impulses were generated when the integrated signal reached a threshold, which was sinusoidally modulated by respiratory activity. B: Linear regression of the respiration-to-heart-rate ratio against the serial correlation coefficient of ΔRR. C: Second-order Poincaré plots illustrating the shift from positive to negative serial correlation as breathing rate increased and/or heart rate decreased, with ring-like patterns emerging at intermediate parameter values.

Discussion

The present findings build upon the classical Poincaré analysis of HRV, as established in prior research (Brennan et al. 2002; Kamen et al. 1996; Khandoker et al. 2013; Raetz et al. 1991; Tulppo et al. 1996; Voss et al. 2009), by introducing a second-order Poincaré plot in which ΔRR_i is plotted against ΔRR_{i+1}. This extension aligns naturally with the existing framework, given that interpretations of Poincaré plots are fundamentally rooted in the statistical properties of ΔRR. The visualization and quantification of serial dependencies in ΔRR thus provide a coherent and meaningful advancement of the methodology.

In the present study, the introduction of the second-order Poincaré plot improved the analysis of cardiorespiratory coupling—the physiological interplay between breathing rhythms and heart rate modulation. Respiration influences cardiac activity through well-established neural mechanisms, particularly respiratory sinus arrhythmia, characterized by heart rate acceleration during inspiration and deceleration during expiration (Berntson et al., 1993; Larsen et al., 2010; Yasuma & Hayano, 2004). Analysis of individual data revealed distinct coupling patterns, with some participants exhibiting pronounced ring-like structures in the second-order Poincaré plots, while others displayed varying degrees of serial correlation in ΔRR intervals. Cross-spectral analysis confirmed respiratory modulation in all cases. We proposed that breathing frequency relative to heart rate determines the observed individual differences: slower respiration produces sustained directional changes in successive RR intervals, yielding positive serial correlations, whereas faster breathing induces more frequent reversals in interval dynamics, leading to negative correlations. This hypothesis was tested using a simple integrate-and-fire oscillator model, where respiration modulated threshold crossings. This model supported the notion that respiratory frequency shaped the temporal structure of HRV, as captured by second-order Poincaré analysis.

Here we analyzed a single data set—the recordings from healthy individuals lying quietly in bed. Under these conditions, respiratory modulation of heart rate is likely to be especially prominent. It would be informative to extend our analysis to other conditions in which first-order Poincaré analysis has been applied previously, for example heart-rate recordings during different breathing regimes (Guzik et al. 2005; 2007), during exercise (Mourot et al. 2004), and in studies of autonomic influences such as head tilts and pharmacological agents (Kamen et al. 1996; Karmakar et al. 2011). It would also be of interest to determine whether second-order Poincaré plots offer additional utility for clinical cases like arrhythmias, where first-order analysis has already been used (Zhang et al. 2015).

In conclusion, our results underscore the value of second-order Poincaré analysis for uncovering dynamical features that conventional HRV metrics may miss. Future research should examine whether similar patterns occur in other physiological oscillator systems and how these dynamics change across different physiological and cognitive conditions, disease states, or pharmacological interventions. The potential clinical applications warrant further exploration, particularly for conditions involving autonomic dysfunction or impaired cardiorespiratory coupling.

Acknowledgements

The experimental data used for this analysis is available at:
https://physionet.org/content/cebsdb/1.0.0/

References

Berntson, G. G., Cacioppo, J. T., & Quigley, K. S. (1993). Respiratory sinus arrhythmia: Autonomic origins, physiological mechanisms, and psychophysiological implications. Psychophysiology, 30(2), 183-196.

Brennan, M., Palaniswami, M., & Kamen, P. (2002). Do existing measures of Poincare plot geometry reflect nonlinear features of heart rate variability?. IEEE transactions on biomedical engineering, 48(11), 1342-1347.

Calabrese, P., & Lambert-Lacroix, S. (2025). Inspiratory and expiratory sinus arrhythmia in healthy human. Physiological Reports, 13(7), e70245.

Ciccone, A. B., Siedlik, J. A., Wecht, J. M., Deckert, J. A., Nguyen, N. D., & Weir, J. P. (2017). Reminder: RMSSD and SD1 are identical heart rate variability metrics. Muscle & nerve, 56(4), 674-678.

Dalmeida, K. M., & Masala, G. L. (2021). HRV features as viable physiological markers for stress detection using wearable devices. Sensors, 21(8), 2873.

García-González, M. A., Argelagós-Palau, A., Fernández-Chimeno, M., & Ramos-Castro, J. (2013, September). A comparison of heartbeat detectors for the seismocardiogram. In Computing in Cardiology 2013 (pp. 461-464). IEEE.

Goldberger, A., Amaral, L., Glass, L., Hausdorff, J., Ivanov, P. C., Mark, R., ... & Stanley, H. E. (2000). PhysioBank, PhysioToolkit, and PhysioNet: Components of a new research resource for complex physiologic signals. Circulation [Online]. 101 (23), pp. e215–e220. RRID:SCR_007345.

Grässler, B., Thielmann, B., Böckelmann, I., & Hökelmann, A. (2021). Effects of different exercise interventions on heart rate variability and cardiovascular health factors in older adults: a systematic review. European Review of Aging and Physical Activity, 18(1), 24.

Guzik, P., Piskorski, J., Krauze, T., Schneider, R., Wesseling, K. H., Wykretowicz, A., & Wysocki, H. (2005). The influence of changing respiratory rate on HRV is portrayed by descriptors of Poincaré plot analysis. Folia Cardiol, 12, 17-20.

Guzik, P., Piskorski, J., Krauze, T., Schneider, R., Wesseling, K. H., Wykretowicz, A., & Wysocki, H. (2007). Correlations between the Poincaré plot and conventional heart rate variability parameters assessed during paced breathing. The Journal of Physiological Sciences, 57(1), 63-71.

Kamen, P. W., Krum, H., & Tonkin, A. M. (1996). Poincare plot of heart rate variability allows quantitative display of parasympathetic nervous activity in humans. Clinical science, 91(2), 201-208.

Karmakar, C. K., Khandoker, A. H., Voss, A., & Palaniswami, M. (2011). Sensitivity of temporal heart rate variability in Poincaré plot to changes in parasympathetic nervous system activity. Biomedical engineering online, 10(1), 17.

Kemp, A. H., & Quintana, D. S. (2013). The relationship between mental and physical health: insights from the study of heart rate variability. International journal of Psychophysiology, 89(3), 288-296.

Khandoker, A. H., Karmakar, C., Brennan, M., Palaniswami, M., & Voss, A. (2013). Poincaré plot methods for heart rate variability analysis (pp. 13-23). New York: Springer.

Kim, H. G., Cheon, E. J., Bai, D. S., Lee, Y. H., & Koo, B. H. (2018). Stress and heart rate variability: a meta-analysis and review of the literature. Psychiatry investigation, 15(3), 235.

Lane, R. D., McRae, K., Reiman, E. M., Chen, K., Ahern, G. L., & Thayer, J. F. (2009). Neural correlates of heart rate variability during emotion. Neuroimage, 44(1), 213-222.

Li, K., Cardoso, C., Moctezuma-Ramirez, A., Elgalad, A., & Perin, E. (2023). Heart rate variability measurement through a smart wearable device: another breakthrough for personal health monitoring?. International journal of environmental research and public health, 20(24), 7146.

Lombardi, F. (2002). Clinical implications of present physiological understanding of HRV components. Cardiac electrophysiology review, 6(3), 245-249.

Mietus, J. E., Peng, C. K., Henry, I., Goldsmith, R. L., & Goldberger, A. L. (2002). The pNNx files: re-examining a widely used heart rate variability measure. Heart, 88(4), 378-380.

Mourot, L., Bouhaddi, M., Perrey, S., Cappelle, S., Henriet, M. T., Wolf, J. P., ... & Regnard, J. (2004). Decrease in heart rate variability with overtraining: assessment by the Poincare plot analysis. Clinical physiology and functional imaging, 24(1), 10-18.

Munoz, M. L., Van Roon, A., Riese, H., Thio, C., Oostenbroek, E., Westrik, I., ... & Snieder, H. (2015). Validity of (ultra-) short recordings for heart rate variability measurements. PloS one, 10(9), e0138921.

Larsen, P. D., Tzeng, Y. C., Sin, P. Y. W., & Galletly, D. C. (2010). Respiratory sinus arrhythmia in conscious humans during spontaneous respiration. Respiratory physiology & neurobiology, 174(1-2), 111-118.

Raetz, S. L., Richard, C. A., Garfinkel, A., & Harper, R. M. (1991). Dynamic characteristics of cardiac RR intervals during sleep and waking states. Sleep, 14(6), 526-533.

Shaffer, F., & Ginsberg, J. P. (2017). An overview of heart rate variability metrics and norms. Frontiers in public health, 5, 258.

Tateno, K., & Glass, L. (2001). Automatic detection of atrial fibrillation using the coefficient of variation and density histograms of RR and ΔRR intervals. Medical and Biological Engineering and Computing, 39(6), 664-671.

Tsipouras, M. G., Fotiadis, D. I., & Sideris, D. (2005). An arrhythmia classification system based on the RR-interval signal. Artificial intelligence in medicine, 33(3), 237-250.

Tulppo, M. P., Makikallio, T. H., Takala, T. E., Seppanen, T. H. H. V., & Huikuri, H. V. (1996). Quantitative beat-to-beat analysis of heart rate dynamics during exercise. American journal of physiology-heart and circulatory physiology, 271(1), H244-H252.

Voss, A., Schulz, S., Schroeder, R., Baumert, M., & Caminal, P. (2009). Methods derived from nonlinear dynamics for analysing heart rate variability. Philosophical Transactions of the Royal Society A: Mathematical, Physical and Engineering Sciences, 367(1887), 277-296.

Yasuma, F., & Hayano, J. I. (2004). Respiratory sinus arrhythmia: why does the heartbeat synchronize with respiratory rhythm?. Chest, 125(2), 683-690.

Zhang, L., Guo, T., Xi, B., Fan, Y., Wang, K., Bi, J., & Wang, Y. (2015). Automatic recognition of cardiac arrhythmias based on the geometric patterns of Poincaré plots. Physiological measurement, 36(2), 283.